CNRS
Centre National de la Recherche Scientifique

INFN
Istituto Nazionale di Fisica Nucleare

Central Interferometer simulations: study of different locking strategies

VIR-0372A-16

Julia Casanueva[1*] and Maddalena Mantovani[2]

[1] *LAL - Laboratoire de l'Accelerateur Lineaire*
[2] *EGO - European Gravitational Observatory*

Date: August 19, 2016

[*] *corresponding author:* casanuev@lal.in2p3.fr

VIRGO* A joint CNRS-INFN Project
Via E. Amaldi, I-56021 S. Stefano a Macerata - Cascina (Pisa)
Secretariat: Telephone (39) 050 752 521 * FAX (39) 050 752 550 * Email: ego@ego-gw.it

Contents

1 Introduction

This note contains the results from the simulations made for the Central Interferometer configuration that is expected to be available for the Advanced Virgo commissioning. The aim is to design a locking strategy (if possible) taking in account the present limitations such as the number of photodiodes, the sensitivity to alignment or to the radius of curvature of the Power Recycling mirror. As it was necessary to consider the impact of alignment and mismatch, all the simulations have been performed with Finesse which is able to include HOMs.

The so called Central Interferometer configuration consists on four main optics: the Power Recycling mirror (**PR**), the Beam Splitter (**BS**) and the input test masses, North Input (**NI**) and West Input (**WI**) as shown in Figure 1. Traditionally this configuration is interesting from the point of view of the commissioning because it allows an initial test of the different subsystems of the interferometer on a less complex system and with a more robust locking scheme.

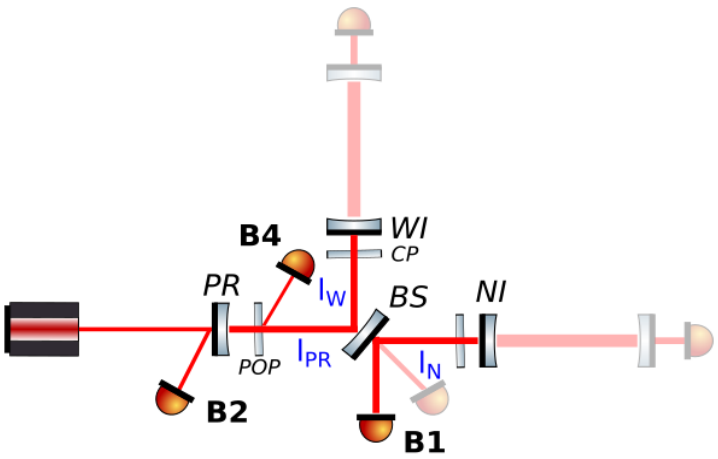

Figure 1: Optical scheme of the CITF configuration available for commissioning. There can be seen the available photodiodes: B1, B2 and B4 as well as the main optics: Power Recycling Mirror, West Input Mirror, North Input Mirror and the Beam Splitter.

In terms of control, there are two longitudinal *Degrees of Freedom* (DOF) on this configuration: the simple Michelson (**MICH**) and the Power Recycling cavity (**PRCL**). The first one is defined as the length difference between the arms, and the second as the length of the power recycling cavity, as shown in Equation 1.1. To lock the interferometer means to control the position of the mirrors in order to keep these two lengths constant at a given value.

$$\begin{aligned} MICH &= |l_{NI} - l_{WI}| \\ PRCL &= l_{PR} + \left(\frac{l_{NI} + l_{WI}}{2}\right) \end{aligned} \tag{1.1}$$

To design a locking strategy means to find a signal for each DOF that contains information about its deviation from the desired length. Then the correction needed to keep the interferometer at the chosen working point is calculated for each DOF, and applied to the mirror actuators. The *driving matrix* provides information about which mirrors need to be moved i order to actuate on each DOF independently. It is worth noting that in principle the actuation for the MICH DOF can be done indifferently with the PR-BS mirrors or with the NI-WI mirrors. In the following the driving is built with the Input mirrors since in simulation, especially with Finesse,

	PR	BS	NI	WI
MICH	0	0	1/2	-1/2
PRCL	1	0	0	0

Table 1: Driving matrix for the CITF configuration. The columns are the mirrors that can be driven and the rows are the two DOFs. It contains information about how apply the correction to the mirrors without affecting the other DOF.

it is more robust to let the BS free. Table 7 shows the driving matrix that will be used.

As the CITF is not the Advanced Virgo final configuration, but a way of testing and debugging the machine, the aim from the point of view of the locking scheme is to control it as robustly as possible. This means there is not a privileged locking configuration. Moreover, as we do not expect to have all the subsystems on their final state, we will make a complete study that would provide us all the information needed to adapt the locking strategy to the actual state of the machine when necessary. Thus two configurations have been studied: one with the Power Recycling cavity locked on the carrier and another one with the Power Recycling cavity locked on the sideband (6 MHz).

2 Status of the CITF simulations

There have already been done simulations on the locking strategy of the CITF [1]. The challenge at that moment was to find a lock strategy with *only one photodiode available* (B2) to control two DOFs. The adopted solution was to use a PDH signal containing information about MICH and PRCL completely decoupled. This means that you could find a demodulation phase where all the information on one DOF is on the in-phase and all the information on the other in the in-quadrature. This ruled out the configuration were the carrier was resonant on the Power Recycling Cavity (PRC), letting as the only possibility to find good error signals to lock the PRC on the sideband instead.

Further studies on the CITF were made on the effect of mirror misalignments on the error signals and proved this to be the limiting factor on the design of the locking strategy. The simulation work done on this topic can be found on the Virgo note [2]. This criticality was expected because the Power Recycling Cavity is marginally stable (only 2 mrad of Gouy phase), and so the Higher Order Modes (HOM) are very close to the resonance and thus amplified. However, the constraints on the initial alignment are highly unlikely to be achieved (the Optical Gain of the error signal drops by 80% on 0.5 μm) so two alternative solutions were proposed:

- The first possibility was to use a *higher demodulation frequency* (131 MHz in our case), which would "see" a lower Finesse of the Power Recycling Cavity, and thus it would be less sensitive to misalignment [2].
- The second one was to *decrease the Radius of Curvature of the PR mirror* in order to improve the cavity stability. This can be done by heating the mirrors using the so called Ring Heater (RH).

The combination of the results of the previous studies, the one on the locking strategy and the one of the impact of the alignment, made the lock of the CITF with only one photodiode very challenging.

3 CITF implementation on Advanced Virgo

Currently the commissioning of Advanced Virgo leaded to a configuration which is different from the one foreseen in the previous Virgo notes thus an update of the locking strategy design is necessary. In particular, the sensing constraints are less stringent because *three photodiodes are now available*: **B1** at the Dark port, **B2** which measures the reflection of the Power recycling cavity (PRC) and **B4** which monitors the intracavity power by

taking a peak-off of the power coming back from the BS using the so called Peak-Off Plate (POP), placed after the PR. Their location is shown on Figure 1.
There are four demodulation frequencies for each photodiode [4] which increases considerably the number of available error signals:

- 62070777 Hz (6 MHz)
- 8361036 Hz (8 MHz): 3 / 4 * 6 MHz
- 56436993 Hz (56 MHz): 9 * 6 MHz
- 131686317 Hz (131 MHz): 21 * 6 MHz

However, this does not reduce the sensitivity to alignment and we expect to be as sensitive on B1 and B4 as in B2. Moreover the solution of using the RH in order to increase the stability of the PRC is not a good option because it is already heating a lot the coils placed on the mirror in order to reach the nominal RoC and further heating would be too risky [3]. The first solution proposed results to be the most promising one and thus will be adopted for this work trying to choose whenever it is possible the error signals demodulated at 131 MHz.

Two possible configurations have been explored: the PRC *locked on the carrier* and the PRC *locked on the sidebands*, 6 MHz, always with the Michelson locked on Dark Fringe. The working point for MICH is given by the minimum of power at the Dark Port (B1) and the working point for PRCL is given by a maximum of power circulating on the cavity (B4), meaning either the cavity or the sidebands are resonant for that length.
In order to determine the working point on the simulation, a scan of each DOF separately has been done, using the driving matrix on Table 7. The scans can be seen on Figure 2.

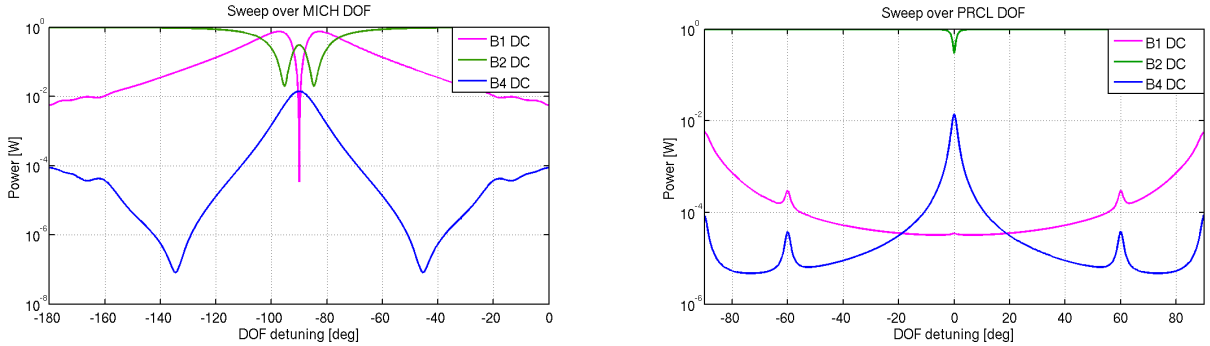

Figure 2: Power on the photodiodes while scanning each DOF. **Left picture:** MICH working point is at -90° of detuning. **Right picture:** PRCL working point for the carrier is at 0° while 6 MHz working point is at ±90°.

The minimum of B1 for the MICH scan can be clearly seen, as well as a maximum on B2 and B4 as expected (when in Dark Fringe all the light goes back towards the injection). In the case of PRCL we can distinguish on B4 the highest resonance at 0° which corresponds to the carrier, as well as two other smaller resonances at 60° and 89.9°. The smallest corresponds to the resonance of the 8 MHz, meanwhile the one at 89.9° corresponds to the resonance of the 6 MHz. This is consistent with the optical design which chose the 6 MHz sideband frequency to be almost antiresonant with respect to the carrier (it is shifted by 300 Hz from anti-resonance).

3.1 Lock strategy definition

For both configurations the best error signal for each DOF has been chosen. This selection process begins by studying all the available error signals, in particular the following parameters:

- **Demodulation Phase:** it has to be tuned in order to optimize the PDH signal either on the *in-quadrature* (Q) or on the *in-phase* (P). Q and P are the projections of the PDH signal onto the real and imaginary

axis respectively. To optimize the projection on one or the other is a matter or convention because it means only a rotation of 90°. In the following the maximization will be performed in the in-phase signal (P).
On the ideal case this means to maximize the slope of the PDH signal but due to the Schnupp asymmetry there is an imbalance of the sidebands that make this task non-trivial (see section 4.1). The strategy adopted was to impose an extra condition: to have a *zero-crossing at or very close to the working point* (which is determined by the position of the resonance for PRCL and of the Dark Fringe for MICH). Once this condition is fulfilled, we select the phase that *maximizes the slope* around the zero-crossing.

- **Linear Region:** a good error signal has to measure how far the DOF is from the working point. This is true on the region where it is linear with respect to the longitudinal displacement and so it is important to have a wide linear range around the resonance.
- **Optical Gain (OG):** the precision of the lock is given by the slope of the error signal. The OG has to be as high as possible in order to maximize the Signal to Noise Ratio (SNR) and so to be more sensitive to deviations from the working point. Notice that the OG value is proportional to the Power and to the finesse.

This information will allow us to discard the error signals that are not valid, such as the ones that do not cross zero at the working point, or those whose linear range is too small compared to the resonance width. However, before choosing the best error signals we need to take in account another factor: the coupling of the DOFs at each demodulated signal.

The **coupling between DOFs** is a crucial issue because the error signals are used to calculate the length correction needed to bring the cavities back to their working point. If the error signal can not decouple the displacement of the two DOFs, the control will over-correct instead of actually control their position.
In order to determine the coupling between DOFs at a given probe, we need to know the optimal demodulation phase for each and the corresponding OG. With this parameters we can build a compass plot that tells us for all demodulation phases how much information from each DOF will be projected on the P and Q signals. Ideally we want them to be completely decoupled, which would mean that for the optimal demodulation phase all the information of PRCL and all the information of MICH is distributed so that a basis where one is entirely in P and the other in Q can be found. In practice this means that their demodulation phases have to be 90° apart. However, if one of the DOFs is completely dominant (its OG is at least one order of magnitude higher than the other) the coupling can be neglected.
At this point we can rule out the probes where the coupling is so high that we can not disentangle the information coming from each DOF. Among all the error signals left, the best would be the one with the higher Optical Gain, although we will try to find a compromise between OG and sensitivity to alignment (higher frequencies are preferred, see section 2). This process will be followed for both CITF configurations: carrier and sidebands.

4 Carrier lock configuration

The first step consists in the optimization of the demodulation phase for all the signals for each DOF to rule out the ones that were not good (no zero crossing at the resonance). Figure 3 shows a scan of both PRCL and MICH, with the suitable error signals and the DC power that gives an idea of the width of the resonance (B4 for PRCL, B1 for MICH), where a linear error signal is needed.

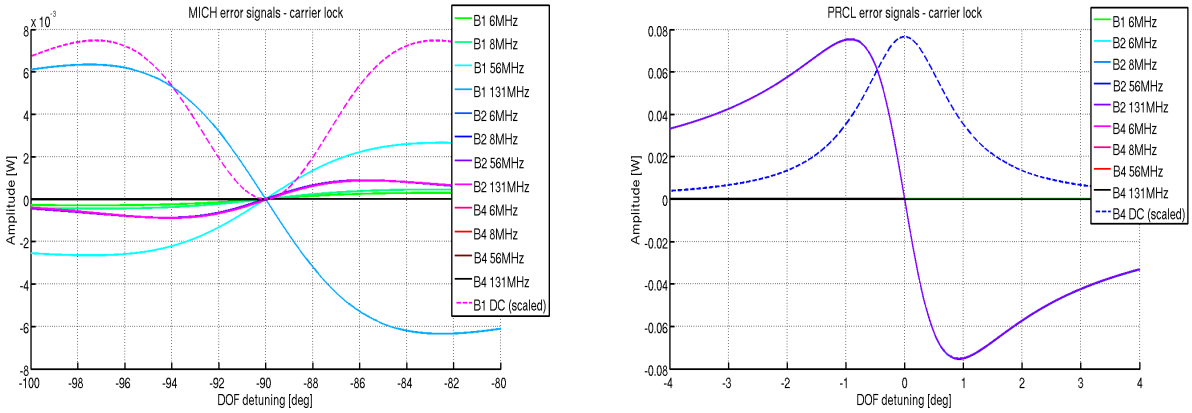

Figure 3: Error signals after optimizing the demodulation phase on P. **Left picture:** MICH scan, the dashed line corresponds to the DC power on the B1 photodiode, showing the working point for this DOF. **Right picture:** PRCL scan, the dashed line corresponds to the DC power on the B4 photodiode, showing the working point for this DOF. Notice that all the error signals from the B2 photodiode are superposed.

In the case of the MICH scan, in principle all the error signals are good candidates. However for PRCL, among all the signals of B1 photodiode only the 6 MHz is a good one as shown in Figure 4. It can be seen that all the other error signals have an horizontal offset, which makes that they do not cross zero at the resonance and which shifts the linear region ($\pm 1°$ in this case).

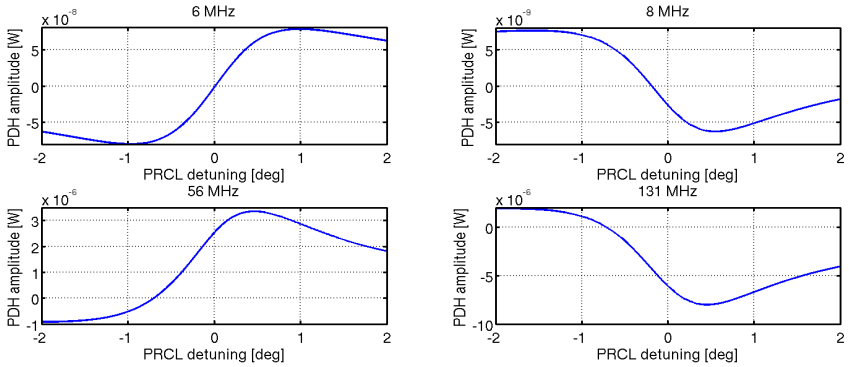

Figure 4: Optimized demodulated error signals at B1 photodiode for a PRCL scan. It can be seen that except for the 6 MHz the zero-crossing is not at zero.

4.1 Cross-coupling

After finding the optimal demodulation phase and thus the corresponding OG, the coupling between the two DOFs for every signal has been evaluated. The corresponding compass plots for all the error signals are shown in Figure 10 in Appendix A.

The outcome of the compass plots shows that on B1 6 MHz, B1 8 MHz, B4 56 MHz and B4 131 MHz the DOFs are completely decoupled, that is, the demodulation phase for each is 90° apart. This means that these signals can be used as error signals for both DOFs, because a basis to decouple the two DOFs can be always found.

All the other error signals are completely coupled, which means that the two DOFs can not be decoupled by tuning the demodulation phase. However, it can be clearly seen that on B1 photo-diode MICH is dominant meanwhile on B2 and B4 photo-diodes is PRCL the dominant one. This is due to the fact that the PRCL is a common DOF while the MICH is a differential DOF.

So even if mixed, the information of the weaker DOF is so small compared to the other one that it can be neglected and these error signals can be used for the dominant DOF.

4.2 Error signals choice

At this point all the information needed to select the best error signal for each DOF is available and it is displayed on Table 2. The error signals in italic are the ones that are decoupled, and the ones in colors are the ones that are completely coupled but there is a dominant DOF (at least one order of magnitude of difference with respect to the other DOF). The cells that are shadowed represent the error signals that have been discarded: in red the ones that did not cross zero at the working point (see previous section), and in gray the ones that were too coupled.

	MICH	PRCL
B1 6MHz	*7.96e-05*	*1.61e-07*
B1 8MHz	*1.22e-04*	*1.32e-08*
B1 56MHz	7.17e-04	3.59e-06
B1 131MHz	**1.71e-03**	8.47e-06
B2 6MHz	3.72e-04	1.63e-01
B2 8MHz	3.72e-04	1.63e-01
B2 56MHz	3.72e-04	1.63e-01
B2 131MHz	3.71e-04	**1.63e-01**
B4 6MHz	5.71e-08	1.42e-05
B4 8MHz	5.62e-08	1.97e-05
B4 56MHz	*1.23e-07*	*2.38e-05*
B4 131MHz	*2.94e-07*	*2.02e-05*

Table 2: Optical Gain for each error signal and each DOF around the working point. The shadowed cells represent the discarded signals. The numbers written in color are the error signals dominating even if coupled. The one in italic are the ones which are decoupled, while the ones in bold are the chosen error signals.

As mentioned previously we wanted the highest optical gain at the highest demodulation frequency (less sensitivity to alignment), which in this case is compatible for both DOFs:

- **MICH sensing will be B1 131 MHz**
- **PRCL sensing will be B2 131 MHz**

B4 131 MHz also fulfills the condition of high demodulation frequency, and on it both DOFs are decoupled, so it could be an alternative option. However, if we take in account that the DC power impinging on the B4 photodiode is smaller (considering the same power arriving to all photodiodes) for PRCL the OG of B4 131 MHz is 3 orders of magnitude smaller on the B2 131 MHz signal (see Appendix B). This applies as well for MICH, where the B4 131 MHz signal would be 7 orders of magnitude smaller than the B1 131 MHz after taking in account the difference on DC power.

The chosen signals are not completely decoupled, but they are dominant over the other DOF as can be seen in Figure 5. First plot shows a sweep of MICH and a sweep of PRCL for B1 131 MHz when its demodulation phase is tunes to optimize MICH DOF. It can be seen that the impact of PRCL is negligible. The second plot shows the same thing for B2 131 MHz optimized for PRCL.

5 Sideband lock configuration

The same process as for the carrier will be repeated, this time for the sideband lock. At first the optimization of the demodulation phase of all error signals for each DOF will be performed, in order to discard the ones

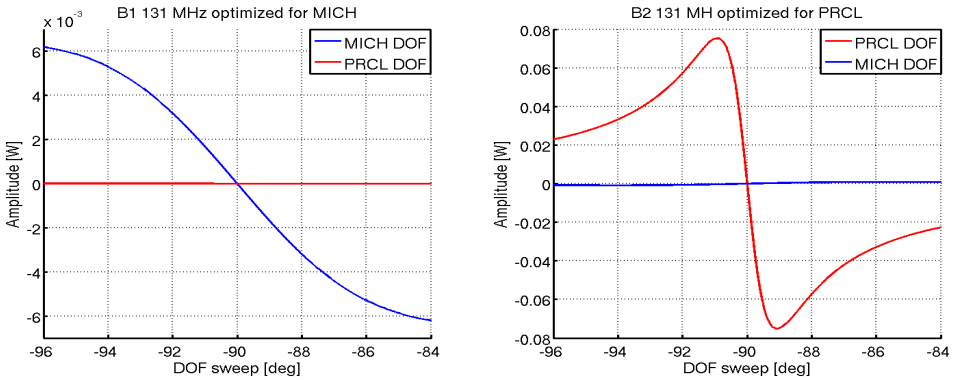

Figure 5: **Left picture:** B1 131 MHz error signal demodulated in order to maximize MICH. In blue a scan of MICH, in red a scan of PRCL. **Right picture:** B2 131 MHz error signal demodulated in order to maximize PRCL. In blue a scan of MICH, in red a scan of PRCL.

that are not good. The remaining error signals are plotted in Figure 6 with the respective DC power providing information about the working point and the resonance width (B1 DC power for MICH and B4 DC power for PRCL).

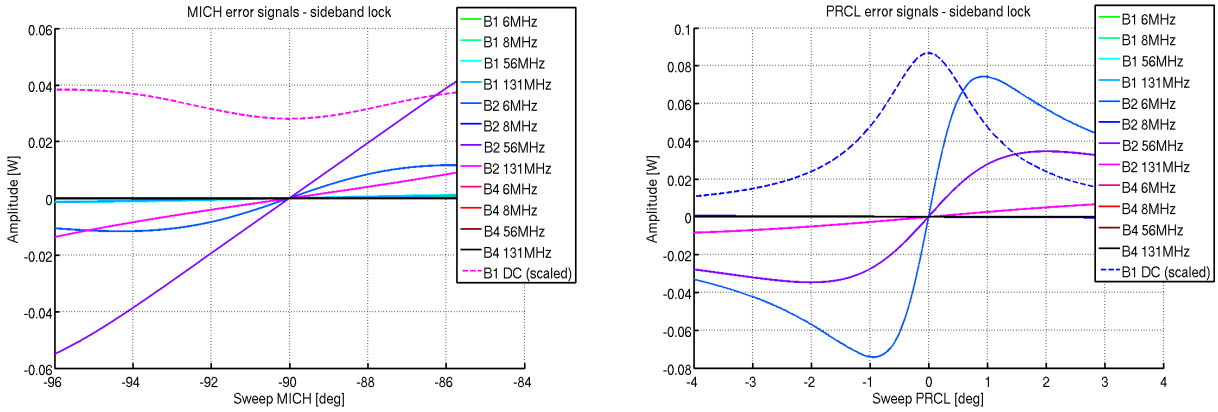

Figure 6: Error signals after optimizing the demodulation phase on P. **Left picture:** MICH scan, the dashed line corresponds to the DC power on the B1 photodiode, showing the working point for this DOF. **Right picture:** PRCL scan, the dashed line corresponds to the DC power on the B4 photodiode, showing the working point for this DOF.

In this configuration all the error signals available are in principle good candidates for both DOFs.

5.1 Cross-coupling

The coupling between both DOFs on each photo-diode has been evaluated like it was done in the previous section for the locking on the carrier. The compass plots containing the information about the couplings are shown in Figure 11 on the Appendi A. As we can see, in this case in all the photo-diodes both DOFs are decoupled so there is no constraint coming from the coupling, we can use all the signals for both photo-diodes.

5.2 Error Signals choice

Table 3 shows all the information about the coupling and the OG of all the error signals. As all the DOFs are decoupled in all error signals, we can choose based only on the criteria of high OG and high demodulation frequency (less sensitivity to alignment). Taking in account both, the best error signal for **PRCL and for MICH is B2 131MHz**. As mentioned on section 2 when the DOFs are decoupled, a basis where the information of both is completely separated can be found and P can be used as error signal for one and Q as error signal for the other.

	MICH	PRCL
B1 6MHz	*7.73e-05*	*1.77e-07*
B1 8MHz	*3.38e-06*	*4.67e-10*
B1 56MHz	*3.31e-04*	*3.26e-06*
B1 131MHz	*2.20e-04*	*1.52e-06*
B2 6MHz	*4.84e-03*	*1.59e-01*
B2 8MHz	*6.88e-06*	*1.27e-04*
B2 56MHz	*9.70e-03*	*3.46e-02*
B2 131MHz	***1.99e-03***	***2.72e-03***
B4 6MHz	*7.29e-07*	*2.36e-05*
B4 8MHz	*1.07e-09*	*2.18e-08*
B4 56MHz	*1.47e-06*	*5.01e-06*
B4 131MHz	*3.01e-07*	*3.60e-07*

Table 3: Optical Gain for each error signal and each DOF around the working point. The signals in italic are the ones decoupled, being the ones in bold the chosen ones.

In case of need we could lock with any of the other 131 MHz error signals, but for the same power impinging on the photodiodes (see Appendix B) the B4 131 MHz has an OG as hig as the B2 131 MHz. In the case of the B1 131 MHz the OG for MICH is one order of magnitude higher while for PRCL is one order of magnitude lower.

6 Carrier vs. sideband: locking strategy

After all this analysis we checked, as expected, that for this CITF configuration a good locking strategy for both lock on the carrier and on the sidebands that fulfils the constraints previously mentioned of using a high demodulation frequency can be found . The only question left is if there is one of the locking strategies (carrier or sideband) to be preferred.

	MICH	PRCL
Carrier	B1 131MHz - 1.71e-03	B2 131MHz - 1.63e-01
Sideband	B2 131MHz - 1.99e-03	B2 131MHz - 2.72e-03

Table 4: For each configuration shows the error signal chosen and its Optical Gain.

Table 4 shows the OG of the error signals chosen for each of the two configurations. It can be seen that for MICH DOF there is almost no difference, meanwhile for PRCL the locking on the carrier shows a SNR of two orders of magnitude larger (larger OG).

It is worth to be noted that in the simulation performed the *the attenuation factor due to the optical benches setup* was not taken in account. This means that the DC considered on each photo-diodes is the one which reach the detection benches. This assumption does not change the coupling between the DOFs, but it has an

impact on the OG. Indeed as mentioned on section 3.1, the Optical Gain scales linearly with the power arriving to the photo-diode thus, knowing the power that impinges on each photo-diode in the simulation, the results can be rescaled to match the actual power on the diodes. This information is displayed on Appendix B.

Also an important factor is the *noise at each photodiode*, which could have a big impact on determining if an error signal can be used or not. Notice as well, that with all the information collected so far, we will be able to look for an alternative locking strategy if any of the error signals is not available at the start of the commissioning.

7 Impact of mismatch on the error signals in a not perfect configuration

So far we have studied what happens on an ideal case, with no HOM included, the beam perfectly matching to the RoC of the PR mirror. However, in reality this will not be the case, because the mirrors will move also angularly introducing a misalignment. As mentioned before, this studies have been done for the CITF when one photodiode was available (see section 2), and we expect the same problems on the other two photo-diodes. The solution proposed was to use a higher frequency, which will be less sensitive to misalignment.

The question we want to address here is the specific situation that we will find at this point of the commissioning. The RH is in charge of heating the PR mirror (which is pre-curved at 1477 m) in order to reach the nominal RoC, 1430 m. However, this creates an additional "thermal lens" effect that will change the RoC of the input beam, which will not be matched anymore. The idea is to compensate this effect by moving the meniscus lens from the Injection bench. The problem is that the dynamics is limited, and even at the end of its range, it does not compensate completely the mismatch.
In principle, this problem will be solved with the so called Central Heating (CH), which uses two gaussian CO_2 lasers to act on the Compensation Plates (they can be seen on Figure 1, just before the Input Test Masses). This way, the CH will induce a thermal lens on the CP that will match the beam to the RoC of the Input Masses.
However the CH will not be ready at this early stage of commissioning, so we try to study the impact of the mismatch that will remain without using the CH. It was estimated that even compensating with the meniscus lens, the RoC of the beam at the PR will be around 1366 m [5]. We checked that in ideal conditions, the mismatch by itself is negligible due to the low finesse of the Power Recycling Cavity (F = 75 for the 6 MHz and F = 1.6 for the 131 MHz [2]). Instead, we studied the impact of the mismatch on the misalignment

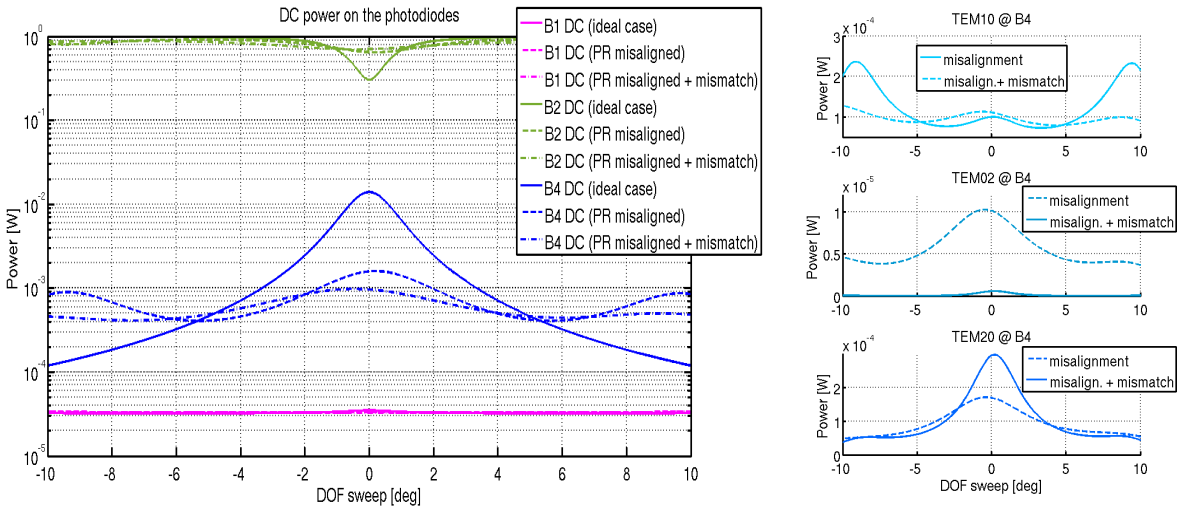

Figure 7: Power on each photodiode during a scan of PRCL in the ideal case, with PR misaligned by 1 μrad and with PR misaligned by 1 μrad plus a mismatch present. On the right it can be seen the power carried by the HOMs on the B4 photodiode for the last two configurations.

7.1 Carrier lock - Effect of misalignment with a mismatch present

In order to study the impact of the mismatch, we compared three scenarios: ideal conditions, PR misaligned by 1 μrad and PR misaligned by 1 μrad with a beam RoC of 1366 m. The difference can be already seen on the DC power arriving to the photodiodes on Figure 7, specially on B4. The misalignment reduces significantly the power circulating on the PRC, and slightly changes the working point (the resonance position is changed). This effect is even more evident when the mismatch is taken in account.

The plot on the right side of Figure 7 shows the power carried by the HOM, which explains the change on the power distribution. Notice as well that the resonance peaks are broader, which means the finesse has decreased. This is due to the power that goes to the HOMs, which do not resonate and is seen by the cavity as losses.

In particular, we are interested on how it affects the error signal, specially the OG. So we repeated the same study as before, optimizing the demodulation phase for each signal and calculating the OG for the two new scenarios: with PR misaligned and with PR misaligned adding a mismatch. All the simulation outcome is shown on Table 5.

It can be seen that for all the error signals the drop of the OG due to a misalignment of 1 μrad is dramatic (more than 90 % in most of the cases). The signals shadowed in red are not taken in account, because they are not good error signals for PRCL (see section 4). In this configuration, with the carrier resonant on the cavity, we do not see any improvement when increasing the demodulation frequency because all the sidebands are almost anti-resonant. They serve only as phase reference, it is only the finesse of the carrier the one that matters here.
Also it is shown on the last column the difference between having a mismatch or not. There is a factor 2.4 of extra OG loss when a mismatch is present.

The carrier lock can be ruled out as a valid configuration for the CITF due to its sensitivity to misalignment.

7.2 Sideband lock - Effect of misalignment with a mismatch present

We repeated the same analysis as in the previous section for the lock on the sidebands. Figure 8 shows the DC power on the photodiodes. We observe the same behaviour as before: power loss on the resonance, appearance

	PRCL ideal	PR misalign.	OG loss (%)	PR misalign.+ mismatch	OG loss (%)	Ratio
B1 6MHz	*1.61e-07*	1.41e-08	91.3	6.53e-09	96.0	2.2
B1 8MHz	*1.32e-08*	2.23e-09	83.1	1.32e-09	90.0	1.7
B1 56MHz	3.59e-06	1.24e-07	96.5	1.30e-07	96.3	0.9
B1 131MHz	8.47e-06	7.65e-08	99.1	7.77e-08	99.1	0.9
B2 6MHz	1.63e-01	1.33e-02	91.8	5.46e-03	96.6	2.4
B2 8MHz	1.63e-01	1.34e-02	91.8	5.48e-03	96.6	2.4
B2 56MHz	1.63e-01	1.33e-02	91.8	5.46e-03	96.6	2.4
B2 131MHz	**1.63e-01**	1.33e-02	91.8	5.45e-03	96.6	2.4
B4 6MHz	1.42e-05	2.03e-06	85.7	8.56e-07	94.0	2.4
B4 8MHz	1.97e-05	2.35e-06	89.1	9.91e-07	95.0	2.4
B4 56MHz	*2.38e-05*	1.99e-06	91.6	8.40e-07	96.5	2.4
B4 131MHz	*2.02e-05*	1.81e-06	91.1	7.59e-07	96.2	2.4

Table 5: Optical Gain for each error signal around the working point when making a scan of PRCL. The first column represents the ideal case as on Table 2, including the information about coupling and the error signal chosen as the most convenient. The shadowed cells represent the discarded signals. The second column corresponds to the configuration with PR misaligned and the third corresponds to the one with PR misaligned plus a mismatch. For each of them the percentage of OG loss is shown. The last column represents the ratio between the losses of both configurations.

of HOM, shift of the working point and broadening of the resonance (decrease on the finesse).

On the right side of Figure 8 we can see the power of the different HOM of the sidebands that are resonant (6 MHz, 56 MHz and 131 MHz). We can notice that the HOM of the 131 MHz have much less power than for the lower demodulation frequencies, as expected. In this case only the HOM of the configuration with PR misaligned are shown, we observe the same effect when a mismatch is present.

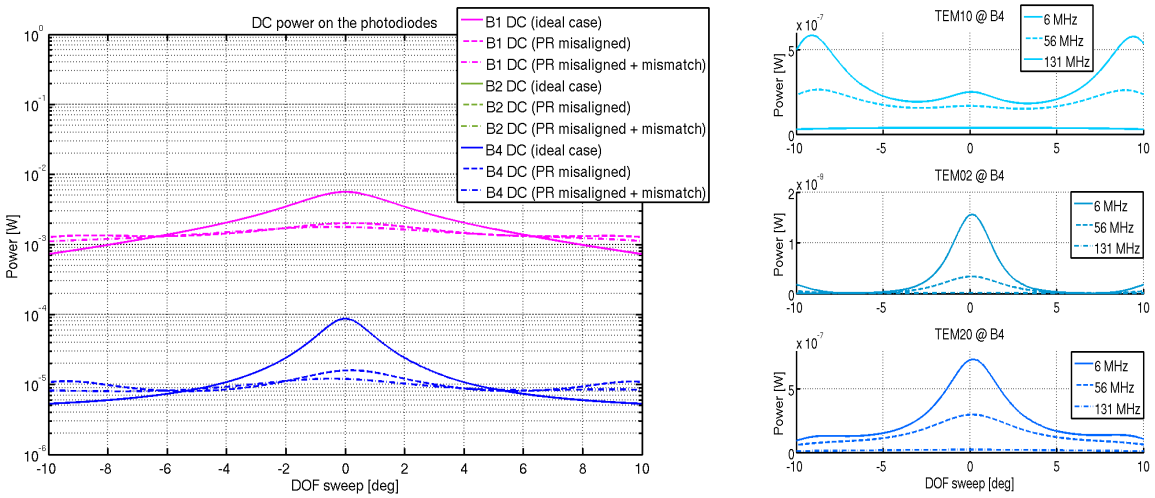

Figure 8: Power on each photodiode during a scan of PRCL on the ideal case, with PR misaligned by 1 μrad and with PR misaligned by 1 μrad and with a mismatch present. On the right it can be seen the power carried by the HOM of each resonant sideband on the B4 photodiode when PR is misaligned but no mismatch is present.

Regarding the OG behaviour when we introduce a misalignment and/or a mismatch, the results are shown on Table 6. The behaviour is very different from what observed for the carrier lock. First notice that the 8 MHz signal increases its OG with misalignment. This behaviour is not well understood yet, however the absolute value is very low that it can be ignored.

Also notice that the OG loss is inversely proportional to the demodulation frequency, so for the 131 MHz the

	PRCL ideal	PR misalign.	OG loss (%)	PR misalign.+ mismatch	OG loss (%)	Ratio
B1 6MHz	*1.77e-07*	1.50e-08	91.5	5.90e-09	96.7	2.5
B1 8MHz	*4.67e-10*	6.53e-10	-39.9	7.15e-10	-53.2	0.9
B1 56MHz	*3.26e-06*	5.52e-07	83.0	3.03e-07	90.7	1.8
B1 131MHz	*1.52e-06*	5.26e-07	65.3	4.42e-07	70.9	1.2
B2 6MHz	*1.59e-01*	1.32e-02	91.7	5.41e-03	96.6	2.4
B2 8MHz	*1.27e-04*	1.73e-04	-36.2	1.85e-04	-45.4	0.9
B2 56MHz	*3.46e-02*	5.63e-03	83.7	3.15e-03	90.9	1.8
B2 131MHz	***2.72e-03***	8.66e-04	68.1	8.16e-04	70.0	1.1
B4 6MHz	*2.36e-05*	2.01e-06	91.5	8.49e-07	96.4	2.3
B4 8MHz	*2.18e-08*	2.99e-08	-37.0	3.29e-08	-50.6	0.9
B4 56MHz	*5.01e-06*	8.35e-07	83.3	4.89e-07	90.2	1.7
B4 131MHz	*3.60e-07*	1.23e-07	65.7	1.19e-07	66.8	1.0

Table 6: Optical Gain for each error signal on the working point when making a scan of PRC. The first column represents the ideal case as on Table 2, including the information about coupling and the error signal chosen as the most convenient.The second column corresponds to the configuration with PR misaligned and the third corresponds to the one with PR misaligned + a mismatch. For each of them the percentage of OG loss is shown. The last column represents the ratio between the losses of both configurations.

loss is significantly lower. This is because of the Schnupp asymmetry. The interference condition of the Michelson depends on the Schnupp asymmetry and the frequency of the sidebands, so the higher the frequency, the more power is leaked to the asymmetric port, which is seen by the cavity as an increase on the losses, thus lowering the Finesse. A low Finesse implies fewer number of round trips on the cavity and so the HOM will be less amplified. This insensitivity to HOM explains why also at higher frequency the impact of an additional mismatch is not significant.

So in this case the 8 MHz can be ruled out because it is not resonant on the cavity and so it is very weak, and the 6 MHz and the 56 MHz because the OG loss is very high. However we can use the 131 MHz for which the mismatch does not have a big impact.

7.3 Carrier vs. sideband: alignment

After this analysis we learned that the carrier lock configuration is not reliable if we expect to have alignment fluctuations. However, the sideband lock is less sensitive to HOMs when demodulating the error signal at a high frequency (in our case at 131 MHz) and so less sensitive to misalignment and mismatch. Thus, the lock on the sidebands is the best option at this point of the commissioning when we expect to have alignment fluctuations and a residual mismatch. B2 photodiode will be used, demodulated at 131 MHz, where after 1 μrad of misalignment we still have 35% of OG. Figure 9 shows a comparison between the chosen error signal for PRCL on ideal conditions, and when a misalignment and a mismatch are present. It can be seen that even if smaller, the error signal is still significant.

8 Conclusion

We have studied the locking strategy of the two possible configurations of the CITF available for commissioning: PRC locked on the carrier and on the sidebands. The performance of all the demodulated signals has been presented for both cases, as well as the impact of the alignment and the mismatch.
The lock on the carrier has been discarded because of its sensitivity to alignment. With a misalignment of 1 μrad there is a loss of the OG around 91% for all the sidebands, which worsens by factor 2.4 when a mismatch is present.

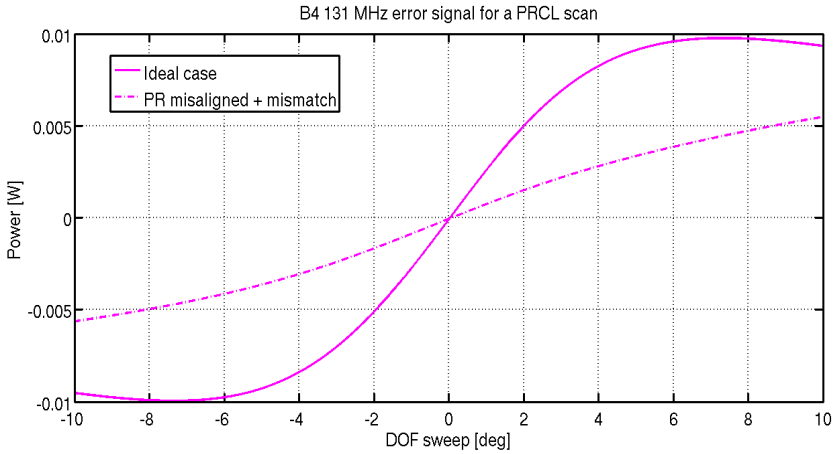

Figure 9: Comparison between PRCL error signal for a sideband lock (B4 demodulated at 131 MHz) on the ideal case and when a misalignment and a mismatch are present.

For the lock on the sidebands the problem of the alignment can be solved by using a high demodulation frequency, 131 MHz. As it has a lower finesse than the other sidebands, it is less sensitive to HOM, and so to misalignment and mismatch. In this configuration after 1 μrad of misalignment there is a loss of the OG of 68%, much lower than on the other cases.
So in the present configuration, the best way to control the CITF is to lock on the sidebands using the P and Q projections of the B2 131 MHz error signal to control the two DOFs. To be veryfied if the noise of the photodiodes will have an impact.
Notice that this effect of insensitivity to HOM for higher demodulation frequencies applies only when the sidebands are resonant. For the CITF where the carrier and the sidebands are anti-resonant this means that to deal with misalignment we have to lock on the sidebands. On the contrary, on the case of the PRITF this will not be a problem because carrier and sidebands are resonant together.

A Compass plots

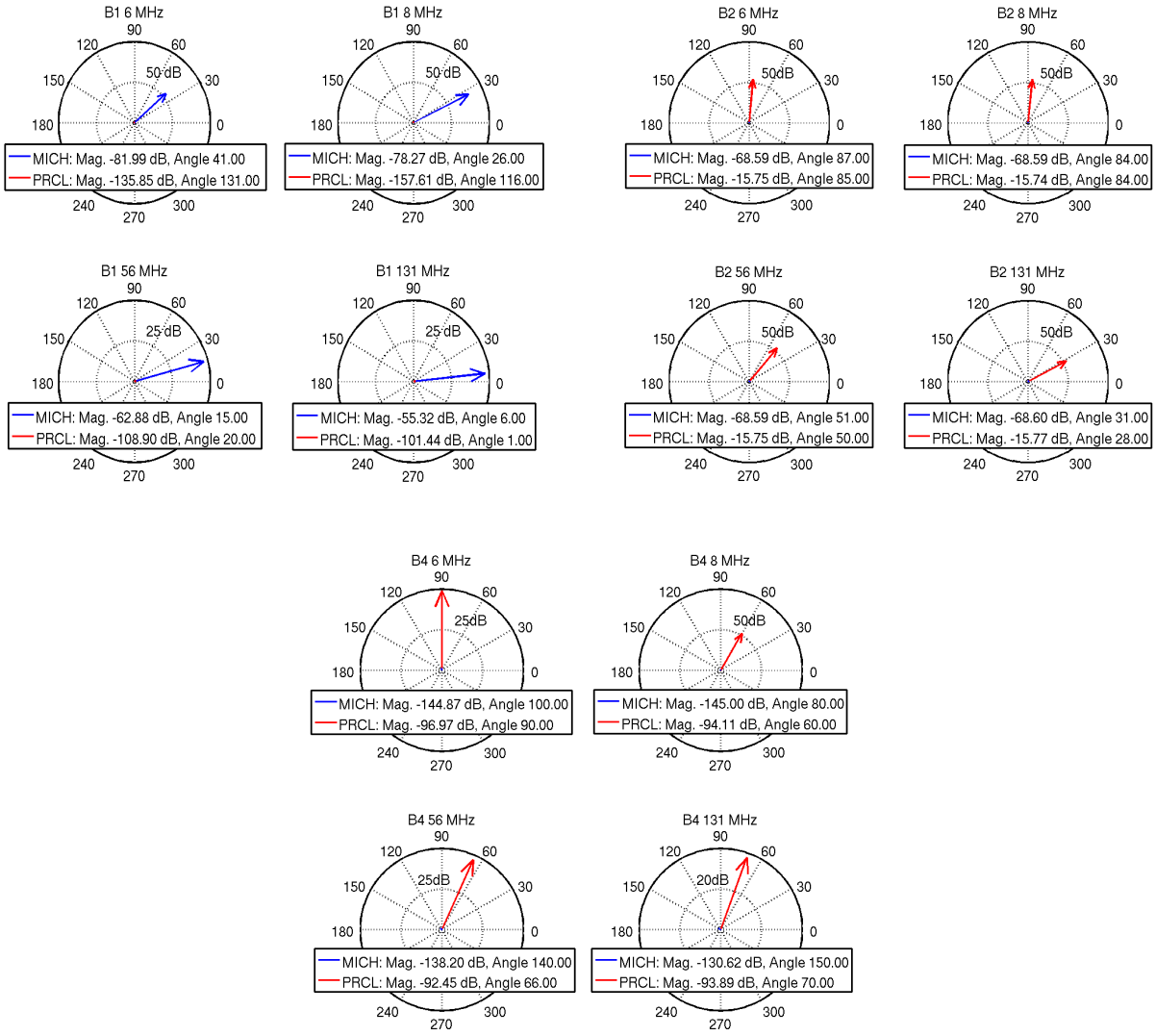

Figure 10: Compass plots showing the cross-coupling of both DOFs when locked on the carrier, in blue MICH and in red PRCL. The magnitude, in dB, represents the Optical Gain and the angle the demodulation phase. Notice that in the legend reads the actual value of the Optical Gain but on the plot the magnitudes are normalized to the smaller one which is fixed to 1dB.**Up-Left picture:** B1 photodiode demodulated signals. **Up-Right picture:** B2 photodiode demodulated signals. **Down picture:** B4 photodiode demodulated signals.

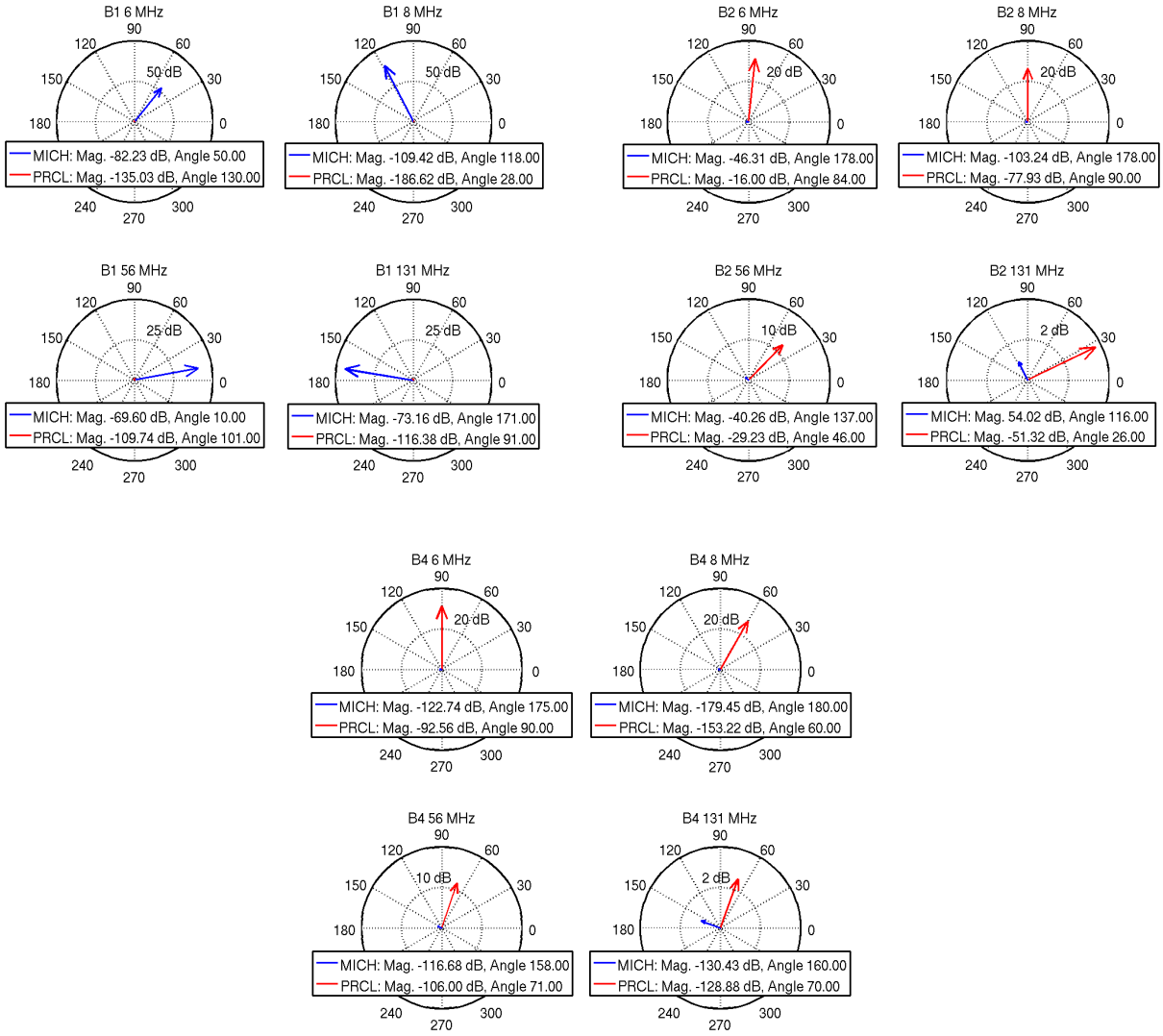

Figure 11: Compass plots showing the cross-coupling of both DOFS when locked on the sideband, in blue MICH and in red PRCL. The magnitude, in dB, represents the Optical Gain and the angle the demodulation phase. Notice that in the legend reads the actual value of the Optical Gain but on the plot the magnitudes are normalized to the smaller one which is fixed to 1dB.**Up-Left picture:** B1 photodiode demodulated signals. **Up-Right picture:** B2 photodiode demodulated signals. **Down picture:** B4 photodiode demodulated signals.

B Optical Gain dependence on DC power

As any attenuation factor of the optical detection benches has been considered, and the OG depends on the power impinging on the photodiodes, Table 7 shows the amount of power arriving to each photodiode on both configurations. This will allow us to recalculate the OG and adapt the locking strategy if necessary. Notice that in principle the photodiodes will be adjusted in order to have the same power arriving to each of them (50 mW) at the final state (with the whole interferometer locked and 125 W of input power).

	Carrier	Sideband
B1 power (W)	3.42e-05	5.62e-03
B2 power (W)	3.03e-01	9.80e-01
B4 power (W)	1.40e-02	8.66e-05

Table 7: Power impinging on each photodiode when locked on the carrier and on the sideband.

References

[1] M. Prijatelj and B. Swinkels, "ISC - simulations regarding locking of the CITF", VIR-0274A-15 (2015). 3

[2] A. Allocca, A. Chiummo and M. Mantovani, "Locking strategy for the Advanced Virgo Central Interferometer", VIR-0187A-16 (2016). 3, 10

[3] A. Allocca, E. Genin, M. Mantovani and B. Swinkels, "Thermal effect of the Ring Heater in the Power Recycling Mirror", VIR-0183A-16 (2016). 4

[4] The Virgo Collaboration, "Advanced Virgo Technical Design Report", Optical Simulation and Design (section 2.3). 4

[5] Personal communication with E. Genin 10